PCCP

Accepted Manuscript

ROYAL SOCIETY OF CHEMISTRY

www.rsc.org/pccp

Bistable electrical switching and nonvolatile memory effect in carbon nanotube-poly(3,4-ethylenedioxythiophene): poly(styrenesulfonate) composite films

Yanmei Sun[1,3], Lei Li[1], Dianzhong Wen[1]*, Xuduo Bai[2]* Gang Li[1]

1 HLJ Province Key Laboratories of Senior-education for Electronic Engineering, Heilongjiang University, Harbin, 150080, China

2 School of Chemistry and Materials Science, Heilongjiang University, Harbin, 150080，China

3 Communication and Electronics Engineering Institute, Qiqihar University, Qiqihar 161006, China

E-mail:sym791122@163.com, wendianzhong@hlju.edu.cn*, xuduobai@hotmail.com*

ABSTRACT The electrical conductance switching behavior and nonvolatile memory effects in poly(3,4-ethylenedioxythiophene):poly(styrenesulfonate) PEDOT: PSS and single-wall carbon nanotubes (SWCNTs) composite thin films have been investigated. The effect of doping level on electrical conductance switching behavior of an indium tin oxide/PEDOT: PSS+SWCNTs/aluminum (ITO/PEDOT: PSS+SWCNTs/Al) sandwich structure has been reported. The ITO/(PEDOT: PSS+SWCNTs)/Al devices show current bistability. Moreover, the ON/OFF state current ratio is in extent of 10^2-10^4. The OFF state current has increased with the decreased SWCNTs content in the composite film, and the ON/OFF state current ratio of the device increases with the increase in SWCNTs content of the composite film. Thus, by varying the doping level of SWCNTs in PEDOT: PSS composite thin films, the electrical conductance switching behavior of ITO/PEDOT: PSS+SWCNTs/Al can be modulated in a controlled manner.

KEYWORDS: carbon nanotube, PEDOT: PSS, WORM, memory, conductance switching

1. Introduction

Organic electronic is a hopeful alternative to the traditional semiconductor devices.[1,2] Over the years, memory devices based on organic nanocomposites have appeared as promising candidates for the next generation of memory devices.[3,4] The organic memory is based on the high and low conductivity response of the device to external applied voltage, making these devices suitable for applications in random access memories. Organic electronic memories exhibit structural simplicity, good scalability, high mechanical flexibility, and low fabrication cost, making them a promising alternative or complementary technology to the inorganic semiconductor information technology.[5,6]

In recent years, polymeric materials and their composites with carbon nanotubes have obtained wide applications in organic electronics.[7-12] Carbon nanostructures have been extraordinarily attractive because of their application in a wide range of organic devices. Among reported organic memory devices, some of them are based on carbon structures embedded in a polymer matrix.[7,8] In memory devices, carbon nanocomposites have been used as charging and discharging islands. Memory behavior has been improved by adding carbon nanostructures such as carbon nanotubes in organic films like poly(*N*-vinyl carbazole) (PVK)[7], 4-triphenylamino-2,6-bis(phenyl)pyridine (F12TPN)[8], poly-4-vinyl-phenol (PVP)[9], poly(3,4- ethylenedioxythiophene): poly(styrenesulfonate), PEDOT: PSS[10,11] polyvinyl alcohol (PVA)[12]. Such devices present reversible or irreversible resistance switching characteristics, depending on case, being potentially useful in volatile or nonvolatile memory devices, respectively. Some reports have shown that doping a polymer matrix with multi-walled carbon nanotubes, MWCNTs at 1 wt.% can improve the performance of WORM memories;[6,12] meanwhile a flash memory behavior is observed in devices with MWCNTs contents of 2 wt.%[5] or 3 wt.%[12]. Furthermore, some studies shown the volatile memory behavior at a small quantity (≤0.01 wt.%) of MWCNTs.[10]

In light of many noticeable works on electrical switching and memory effects in doped or mixed polymer systems,[13-15] the impact of doping level on the electrical switching behavior of polymeric systems seemingly should be further explored. It is reasonable to look forward to that doping levels will

noticeably affect charge transport processes in the bulk and at the interface and will have a significant influence on device performance.[16]

Although many carbon nanotubes-based resistance random access memory devices have been explored,[7-12] the certain properties of the composite based on carbon nanotubes has not been found. Compared with MWCNTs, single-wall carbon nanotubes (SWCNTs) have small diameter, less defect and a higher uniform consistency, which is beneficial to miniaturization and stability of memory device. In this work, the electrical conductance switching behavior and nonvolatile memory effects in PEDOT: PSS and SWCNTs composite thin films have been observed. The effect of SWCNTs doping level on electrical conductance switching behavior of ITO/(PEDOT: PSS+SWCNTs)/Al devices also has been reported. The ON/OFF state current ratio of the WORM device increases with the increase in SWCNTs content of the composite film. The electrical and bistable switching behaviors of the PEDOT: PSS+SWCNTs composite films can be tuned by modulating the SWCNTs content (doping level) in the composite films.

2. Experimental details

2.1 Materials

The PEDOT: PSS (2.8 wt% dispersion in H_2O) was provided by Sigma-Aldrich. The SWCNTs were purchased from NanoLab Inc. (Newton, MA). The outer diameter, length, specific surface area, and purity of the SWCNTs were 1-2 nm, 5-30 μm, 450 m^2/g, and 95%, respectively. Transmission electron microscopy (TEM) measurements were carried out to investigate the micro-structural properties of those SWCNTs, as shown in Fig. 1.

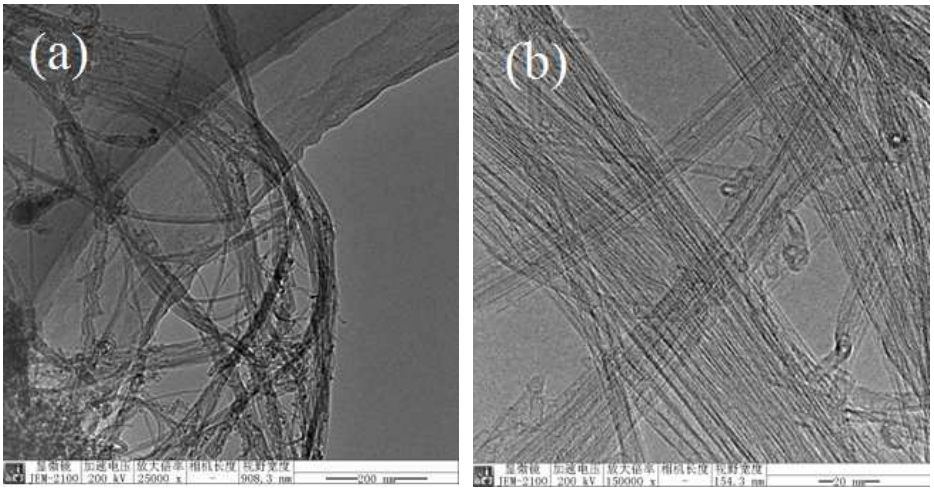

Fig. 1 TEM of SWCNTs (a) Low resolution (b) High resolution

The FTIR spectra was used to analyze the presence of bond in SWCNTs. Fig. 2 shows FTIR spectra of SWCNTs which tested by Foss DS 2500 infrared spectrometers. It exhibits a characteristic absorption peak at 3396 cm^{-1}. This peak is attributed to the O-H stretching mode,[17] which probably is associated with hydrocarbon contamination in spectrometer. Further the broad absorption peak at 1520 and 1312 cm^{-1} can be attributed to the stretching of C=C and C-C bonds.[18] Moreover, the peak at 1110 cm^{-1} can be ascribed to the stretching vibration of C-O.[19]

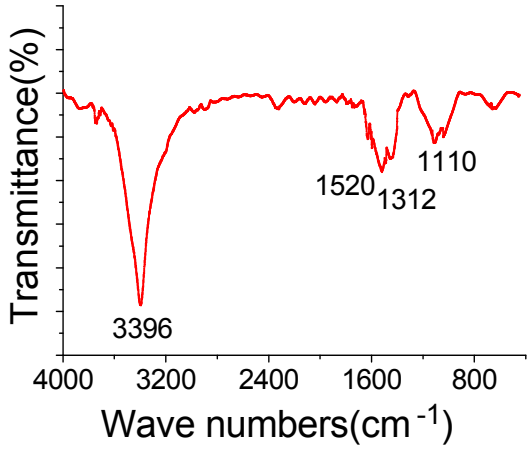

Fig. 2 The FTIR spectra of SCWNTs

2.2 Fabrication and measurement of the memory device

For fabricating the devices, indium tin oxide (ITO) glass of dimensions 2 cm × 1 cm (sheet resistance $R_{\square}$=15 Ω cm^{-1}) were cleaned by ultrasonicating sequentially in detergent, distilled water, acetone, isopropanol and methanol for 20 minutes each. They were then dried in a vacuum oven at 60 ℃ overnight. ITO/(PEDOT: PSS+SWCNTs)/Al devices were prepared on ITO/glass substrates. The PEDOT: PSS+SWCNTs composite was prepared by using the following procedure: the SWCNTs were dissolved in isopropyl alcohol and the dispersion was ultrasonicated for 40 min. After that, the SWCNTs dispersion was mixed with the previously filtered PEDOT: PSS aqueous solution (0.45 μm pore size filter) and ultrasonicated for 1 h. Samples with different concentrations were prepared, as shown in Table 1.

Table 1 Different concentration of the composite films used in each sample

Sample	SWCNT(mg)	Isopropyl alcohol(mL)	PEDOT: PSS(mL)
A	8	1	2
B	5	1	2
C	1	1	2
D	0.3	1	2

Finally, this composite was spin-coated at a spinning speed of 700 rpm for 18 s and then 2000 rpm for 60 s on the ITO electrode and then dried in a vacuum oven at 70 ℃ at a pressure of 100 Pa for 5h. The film thickness was measured with scanning electron microscope (Hitachi S3400). The top Al electrode layer of about 200 nm thickness was thermally evaporated at a base pressure of 1.0×10^{-4} Pa using a shadow mask. The diameter of the top electrode is 200 μm. Structural formulas of PEDOT: PSS and the structure of memory device are shown in Fig. 3. The electrical characterization of the memory device was performed by a Keithley 4200-SCS semiconductor parameter analyzer in an ambient atmosphere using a probe station at room temperature without any encapsulation. A two-terminal current voltage (*I-V*) test was carried out. The bottom electrode (ITO) was grounded during all the electrical measurement with a swept step of 0.05 V.

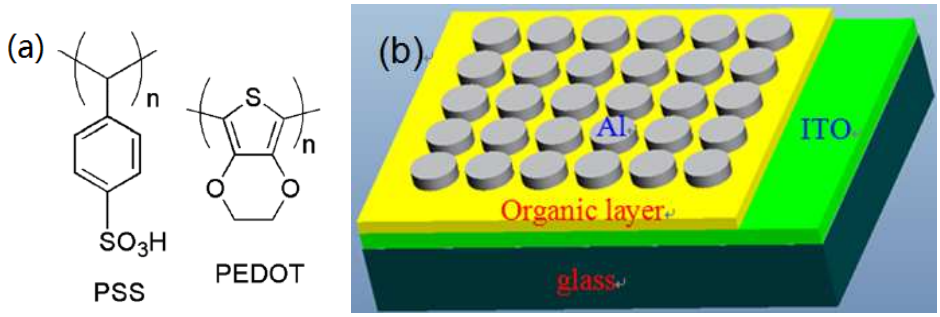

Fig. 3 (a) Structural formulas of PEDOT: PSS (b) Schematic diagram of the ITO/PEDOT: PSS+SWCNTs/Al sandwich devices.

The cross-section scanning electron microscopic (SEM) images of the PEDOT: PSS+SWCNTs composite films before the evaporation of Al electrode are shown in Fig. 4, from the top to bottom is glass, ITO film and PEDOT: PSS+SWCNTs composite film, respectively, the thickness of the different concentration of composite film can be judged as 59.7, 64.6 and 69.4 nm from this image, respectively. As shown in the SEM images, SWCNTs are distributed uniformly in the PEDOT: PSS, and they are well integrated into the polymer matrix, and it is difficult to distinguish individual SWCNTs from the PEDOT: PSS matrix.

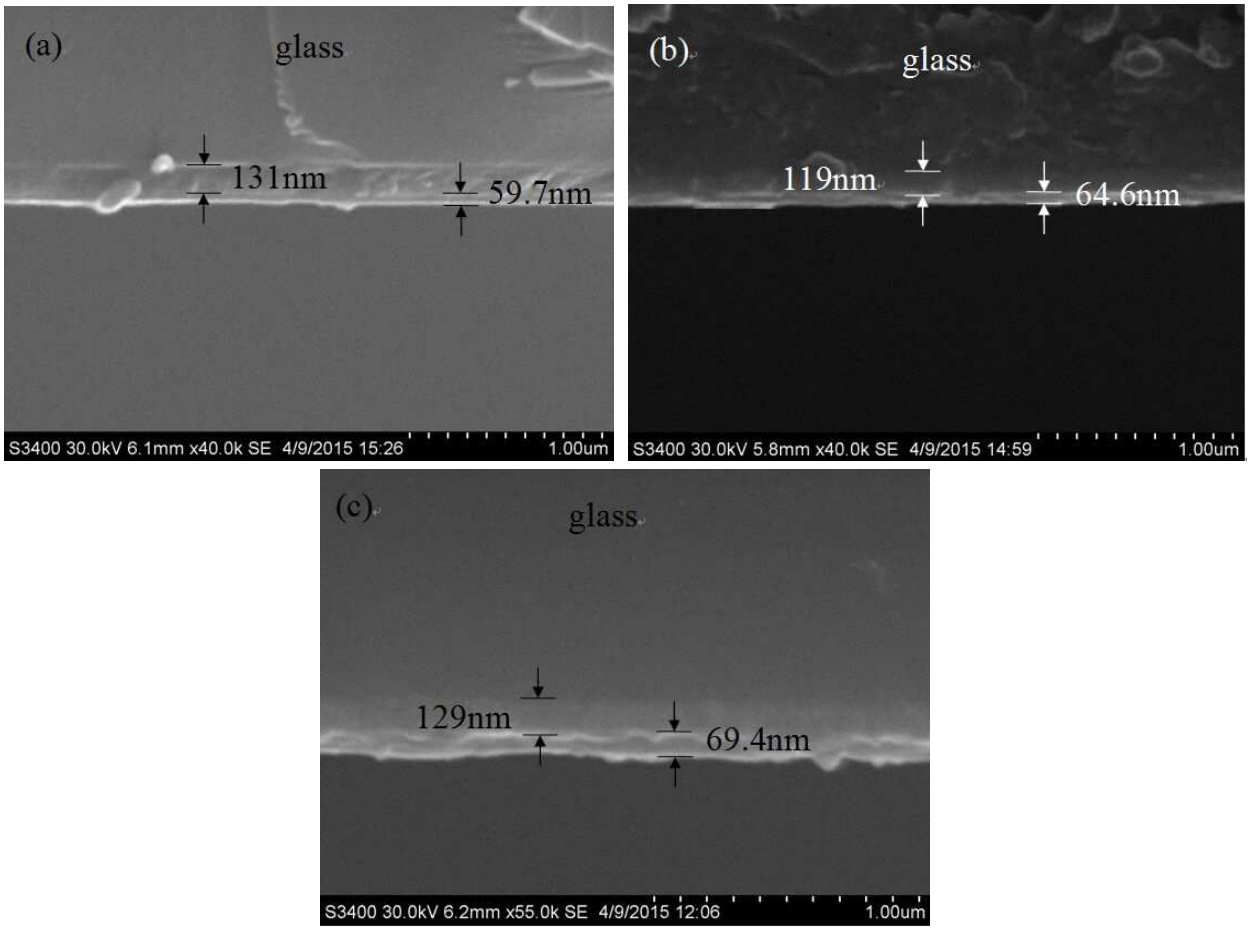

Fig. 4 Cross-section scanning electron microscopic images of the PEDOT: PSS+SWCNTs composite films based on (a) sample A (b) sample B (c) sample C

Fig. 5 shows TEM image of SWCNTs embedded in a PEDOT:PSS layer. The TEM image shows that the SWCNTs are randomly dispersed in the PEDOT:PSS layer. The length of SWCNTs decreases,

resulting from a cutting of the original SWCNTs after ultrasonication. The results indicated that the two composites were well mixed.

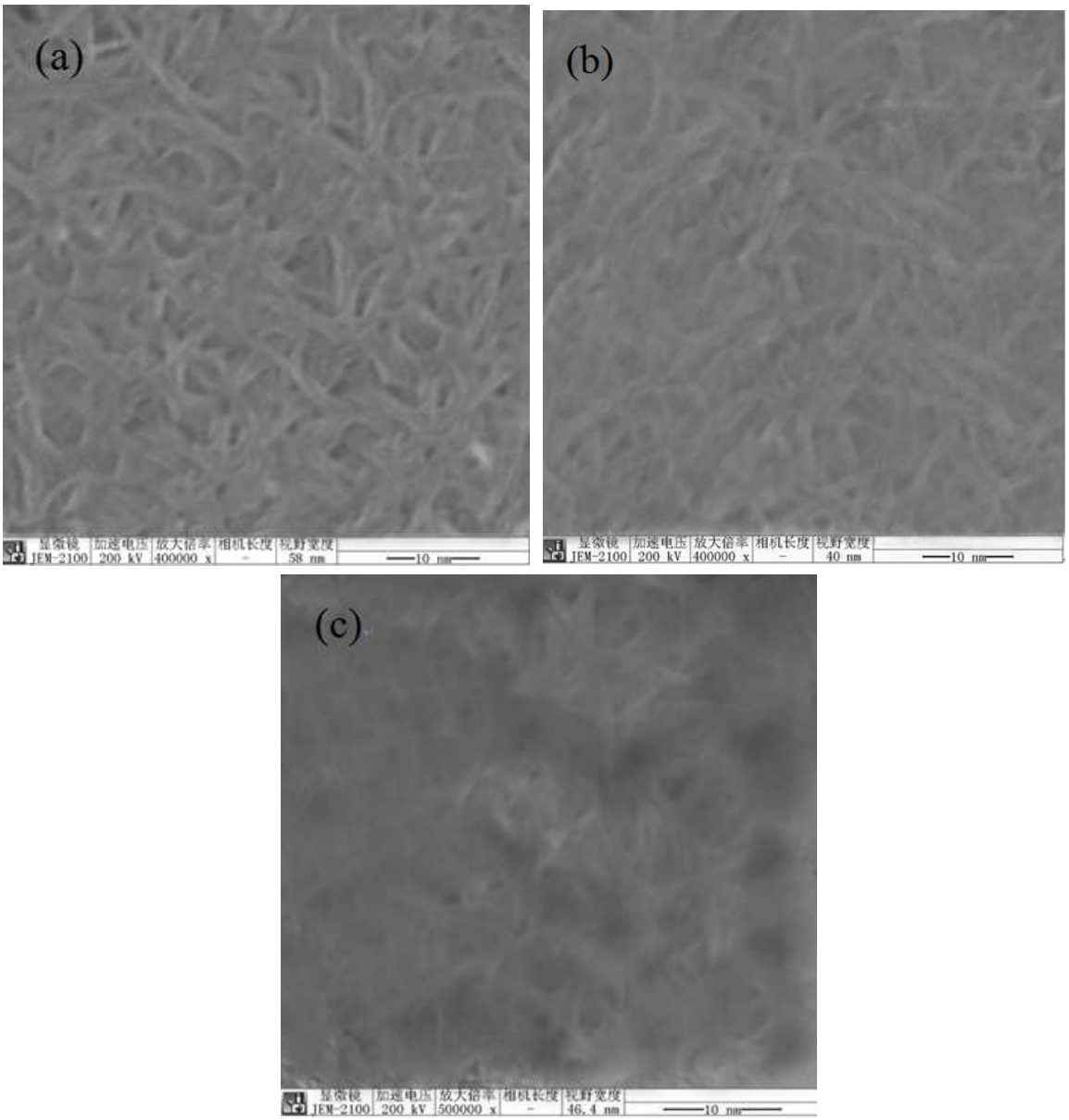

Fig. 5 TEM of SWCNTs embedded in the PEDOT: PSS layer (a) sample A (b) sample B (c) sample C

2.3 Characterization of the PEDOT: PSS+SWCNTs composite material

2.3.1 Thermal properties

The thermal properties of PEDOT: PSS+SWCNTs composite materials were investigated by TGA, The solutions based on different samples were dried in a vacuum oven at 80 □ for 36 h, then the formed film were crushed down for thermal properties analysis. The typical TGA curves of pure PEDOT: PSS and composites materials are depicted in Fig. 6. During the TGA analysis by using the TA instruments Q-50, a ramping rate of 10 □/min was employed. The composites materials exhibited good thermal stability with insignificant weight loss up to 280 ℃ under air atmosphere. The 10% weight-loss temperatures of composites materials was recorded to be 310 ℃, 299 ℃, 294 ℃ and 281 ℃ for the composites materials based on sample A, sample B, sample C and sample D, respectively. The heat resisting property of composites materials are better than pure PEDOT: PSS, which could be ascribed to

the good thermal property of SWCNTs. The excellent thermal properties were advantageous to the memory device which may release heat during operation.

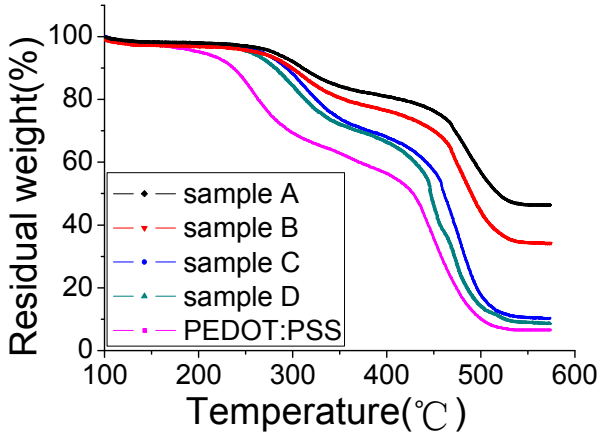

Fig.6 TGA curves of PEDOT: PSS+SWCNTs composite material

2.3.2 The initial resistivity of PEDOT: PSS+SWCNTs film

The initial resistivity of the film was performed by a RTS-9 4-point probes resistivity measurement system, (4 PROBES TECH., CHINA). The results are shown in Fig. 7. The resistivity of film is increased with the decreasing of SWCNT content in PEDOT: PSS matrix, as shown in Fig. 7. From the resistivity of PEDOT: PSS+SWCNTs film, we can see that the composite materials are semiconductors (The resistivity of semiconductor is between 10^{-6} and 10^{8} $\Omega \cdot m$).

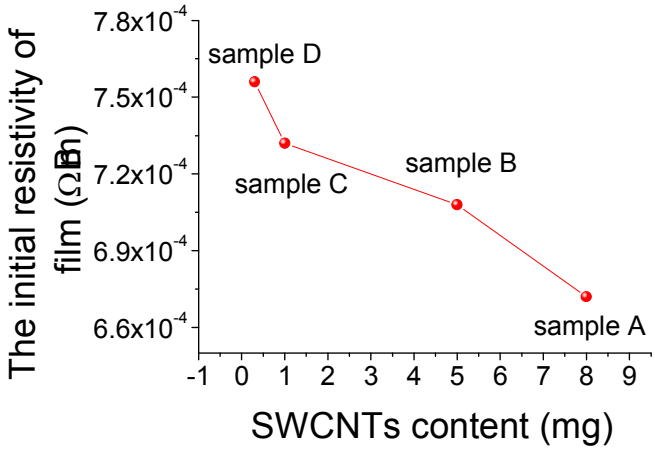

Fig. 7 The initial resistivity of PEDOT: PSS+SWCNTs film

3. Results and discussion

We have changed the SWCNTs concentrations added to PEDOT: PSS solution as shown in table 1. The ITO/PEDOT: PSS+SWCNTs/Al devices with different SWCNTs concentrations, showed basically the same electrical behavior while the devices with small concentration of SWCNTs exhibit a single low conductivity state.

The current-voltage (*I-V*) characteristics of ITO/(PEDOT: PSS+SWCNTs)/Al device based on sample A were shown in Fig. 8. When the top electrode was initially biased "-" relative to the bottom, an external applied voltage was swept from 0 to -8 V, 0 to -8 V and then 0 to 8 V. The devices initially were

in a high conductivity (ON) state. The current increased as the voltage was increased till at a certain value, near -6.05 V, the current slumped abruptly by several orders of magnitude and switched the devices permanently to a low conductivity (OFF) state. Fig. 8(a) shows a typical *I-V* characteristic of the device. The devices were kept in the OFF state for all subsequent sweeps, thus enabling them to be used as write-once-read-many times (WORM) devices.[20] What is noteworthy is that, when the top electrode was initially biased "+" relative to the bottom, the device also showed up WORM memory effect. As shown in Fig. 8(a), an abrupt drop in the current is observed at a switching threshold voltage of 6.85 V when scanning the device firstly with positive bias from 0 to 8 V. Both the ON/OFF current ratio and the switching threshold voltage are comparable in magnitude to those in the negative switching process, indicating the bi-directionally switchable characteristics of the sample A-based memory device.

In order to test the retention performance of the device, the current in ON and OFF states were measured continuously at a read voltage of -4 V with an initial negative voltage sweep, as shown in Fig. 8(b). The device remained ON and OFF states for more than 3.3 h, and the ON/OFF current ratio maintains about 5×10^4 at -4 V. The endurance performance of the device in both ON and OFF states was measured at -4 V pulse (2 ms in period, 1 ms in duration width), as shown in Fig. 8(c). The device exhibited little degradation over 1.2×10^4 cycles with ON/OFF current ratio of over 5×10^4.

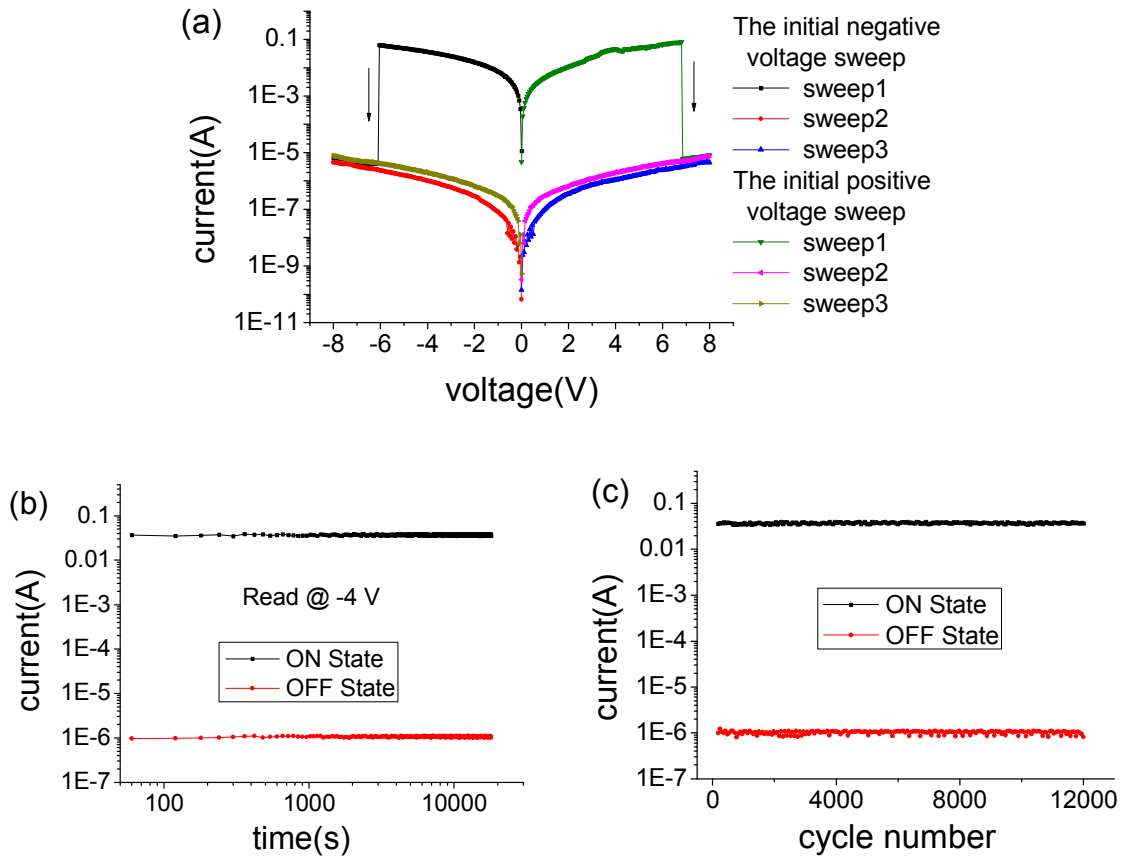

Fig. 8 (a) *I-V* characteristics of the ITO/(PEDOT: PSS+SWCNTs)/Al device based on sample A with an initial negative voltage sweep and an initial positive voltage sweep (b) Retention performance of ITO/(PEDOT: PSS+SWCNTs)/Al device based on sample A with an initial negative voltage sweep. (c) The endurance performance of ITO/(PEDOT: PSS+SWCNTs)/Al device based on sample A with an initial negative voltage sweep.

The *I-V* characteristics of device based on sample B and C are similar to that of sample A, and both

displayed distinctly bistable electrical conductivity states, as shown in Fig. 9 and Fig. 10. A slight increase in the OFF current progressively occurs with the decreased SWCNTs content in the composite film, which not beneficial to the performance of device because it reduces the ON/OFF current ratio, and increases the possibility of misreading.

As shown in Fig. 9(a), the device based on sample B switches at the voltage of -6 V (the negative bias was firstly applied) and 7.10 V (the positive bias was firstly applied) with a slightly lower ON/OFF state current ratio of about 5×10^3 and exhibits similar bi-directionally switchable WORM memory switching behavior. The retention performance of device based on sample B in the ON and OFF state was measured at -4 V with an initial negative voltage sweep, as shown in Fig. 9(b). The ON and OFF state currents can be sustained under a constant voltage stress of -4 V for up to 3.3 h. The endurance performance of device based on sample B in the ON and OFF state was shown in Fig. 9(c). The ON and OFF states of device are stable for up to 1.2×10^4 continuous read pulses of -4 V.

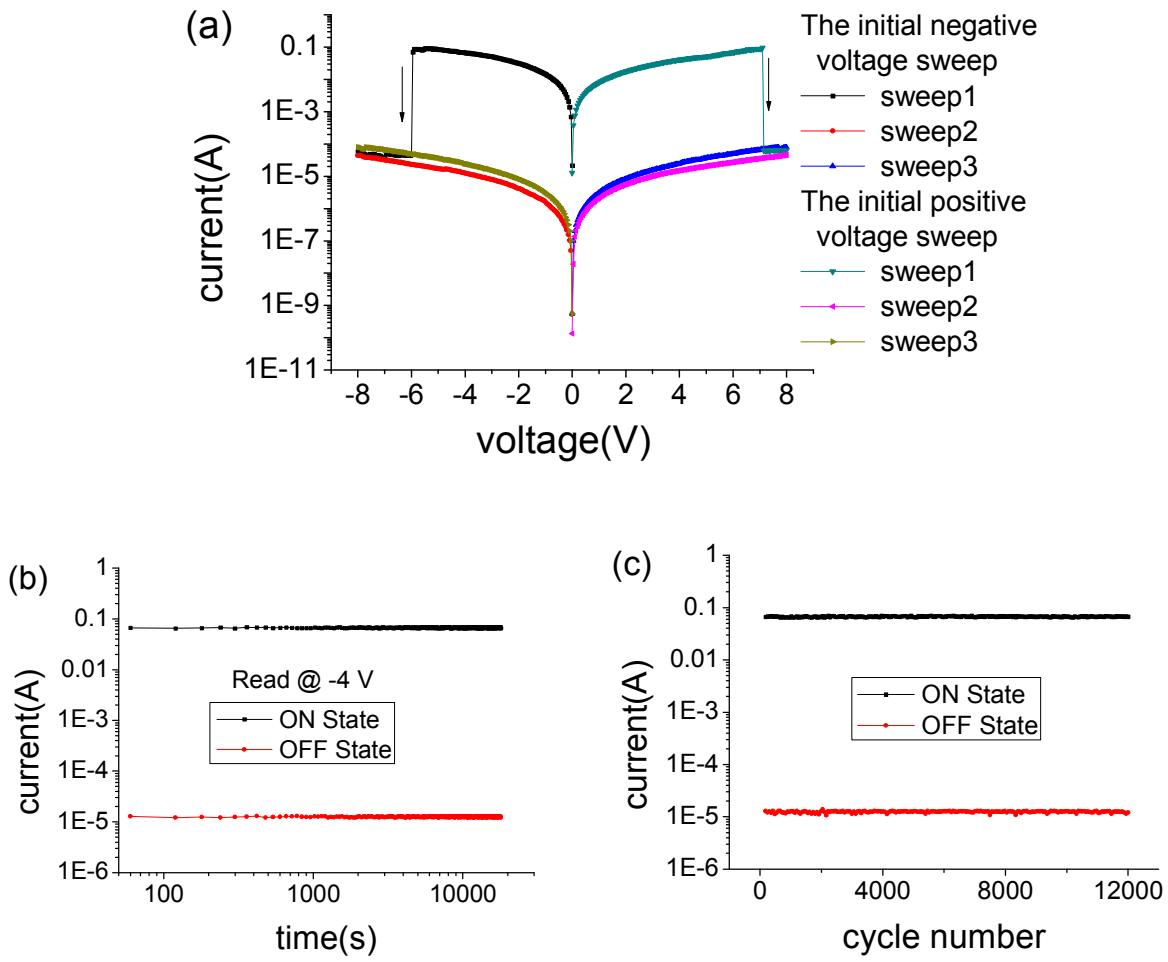

Fig. 9 (a) *I-V* characteristics of the ITO/(PEDOT: PSS+SWCNTs)/Al device based on sample B with an initial negative voltage sweep and an initial positive voltage sweep. (b) Retention performance of ITO/(PEDOT: PSS+SWCNTs)/Al device based on sample B with an initial negative voltage sweep. (c)The endurance performance of ITO/(PEDOT: PSS+SWCNTs)/Al device based on sample B with an initial negative voltage sweep.

The device based on sample C also shows the bi-directionally switchable characteristics. It switches at the threshold voltage of -5.90 V and 7.05 V (as shown in Fig. 10(a)) with a lower ON/OFF state current

ratio of about 2×10^2 at -4 V and exhibits similar WORM memory switching behavior. Fig. 10(b) shows that the ON and OFF states with an initial negative voltage sweep are retained under a constant voltage of -4 V, also used as reading voltage. The measurement was made every 60 s during 3.3 h. The ON/OFF state current ratio larger than two orders of magnitude is observed throughout the measurements. The endurance performance of device based on sample C in the ON and OFF state was shown in Fig. 10(c).

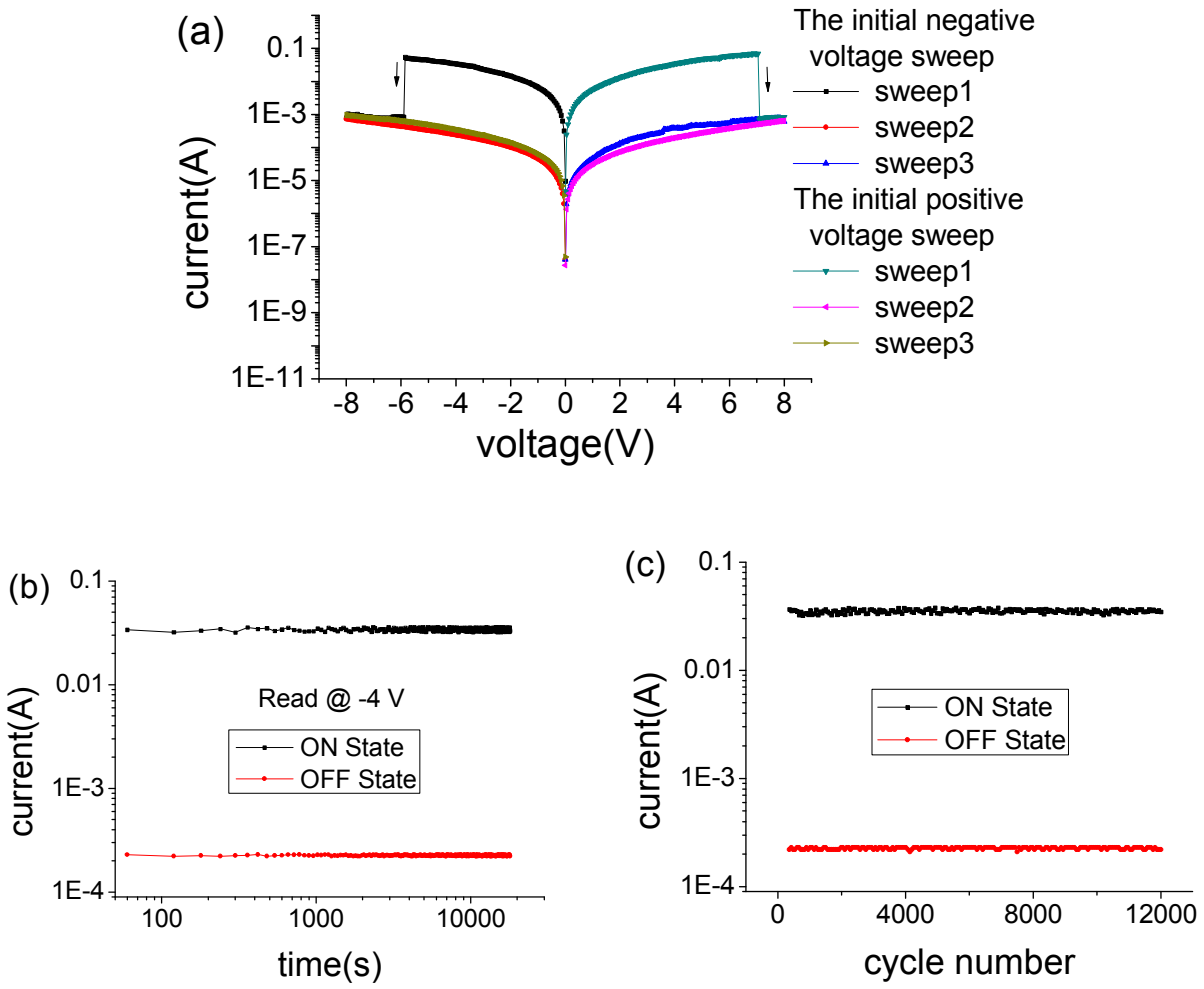

Fig. 10 (a) *I-V* characteristics of the ITO/(PEDOT: PSS+SWCNTs)/Al device based on sample C with an initial negative voltage sweep and an initial positive voltage sweep. (b) Retention performance of ITO/(PEDOT: PSS+SWCNTs)/Al device based on sample C with an initial negative voltage sweep. (c) The endurance performance of ITO/(PEDOT: PSS+SWCNTs)/Al device based on sample C with an initial negative voltage sweep.

Further decrease in SWCNTs content results in a obvious increase in the conductivity of the composite film, and devices based on sample D exhibit a single state conductor behavior, as shown in Fig. 11.

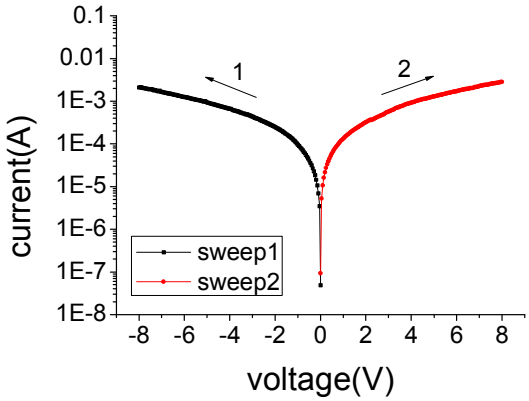

Fig. 11 *I-V* characteristics of the ITO/(PEDOT: PSS+SWCNTs)/Al device based on sample D

The effect of SWCNTs content in the composite films on device performance, including the OFF state current under a given voltage (-4 V) and ON/OFF state current ratio, is summarized in Fig. 12. The electrical conductivity in OFF state of the composite films is decreased by 3 orders of magnitude with the increase in SWCNTs content. The ON/OFF state current ratio increases by 4 orders of magnitude, as the SWCNTs content is increased.

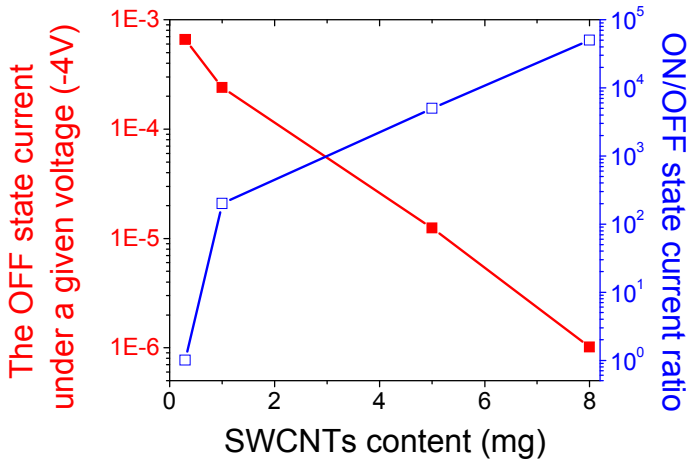

Fig. 12 The OFF state current (absolute value) under a given voltage of -4 V and ON/OFF state current ratio of the ITO/(PEDOT: PSS+SWCNTs)/Al devices.

The current of OFF state increased obviously and ON/OFF state current ratio reduced with the decrease of doping amount for SWCNTs, thus the process of resistive switching may be different. In order to further understand the reason why OFF state current increased and ON/OFF state current ratio decreased with the decrease of doping amount for SWCNTs, we investigated the *I-V* characteristics of both ON state and OFF state in details by using log-log plotting and the corresponding linear fitting. The measured *I-V* characteristics of the devices were further analyzed in detail with various conduction models to investigate their electrical switching characteristics. In the log-log scale, the slope of a fitted line is actually the exponent in the relationship between the current and the voltage, which contains the information of transport mechanism of both ON state and OFF state.

Fig. 13 shows the *I-V* curves in log-log scale for ON and OFF state with an initial negative voltage sweep. In order to better fit the slope and find out the most appropriate relationship between current and

voltage, in general, the slope of certain conductance state is divided into two parts to carry on the fitting. As shown in Fig. 13, for all high conductivity state of the devices based on the different samples, Ohm's relationship supported by thermal carrier generation can be observed. *I-V* curves were linear fitted with a slope of 1.02, 1.06, 1.07 and 1.09. The slopes were very close to 1. This means that the relationship between current and voltage of the high conductivity state obeys the well-known Ohm's law and conductive pathways were formed. Then for the low conductivity state of the devices, curves become steeper, and the slopes of devices are larger than 1 (1.82, 1.54, 1.22 and 1.40). According to the trap-controlled space charge limited conduction (SCLC) theory, this is the region that obeys the Child's law in the presence of shallow trapping.[3] Charge accumulation process occurred in this progress. This occurs probably due to the creation of trap states at the metal-organic semiconductor interface. Here Al atoms diffused into the PEDOT: PSS+SWCNTs layer during thermal evaporation of the top Al electrode leading to the formation of donor impurity band for current conduction. Hence energy band bending occurs at the metal-semiconductor heterojunction due to the trapped electrons. These findings are reported to be consistent with that found earlier.[21]

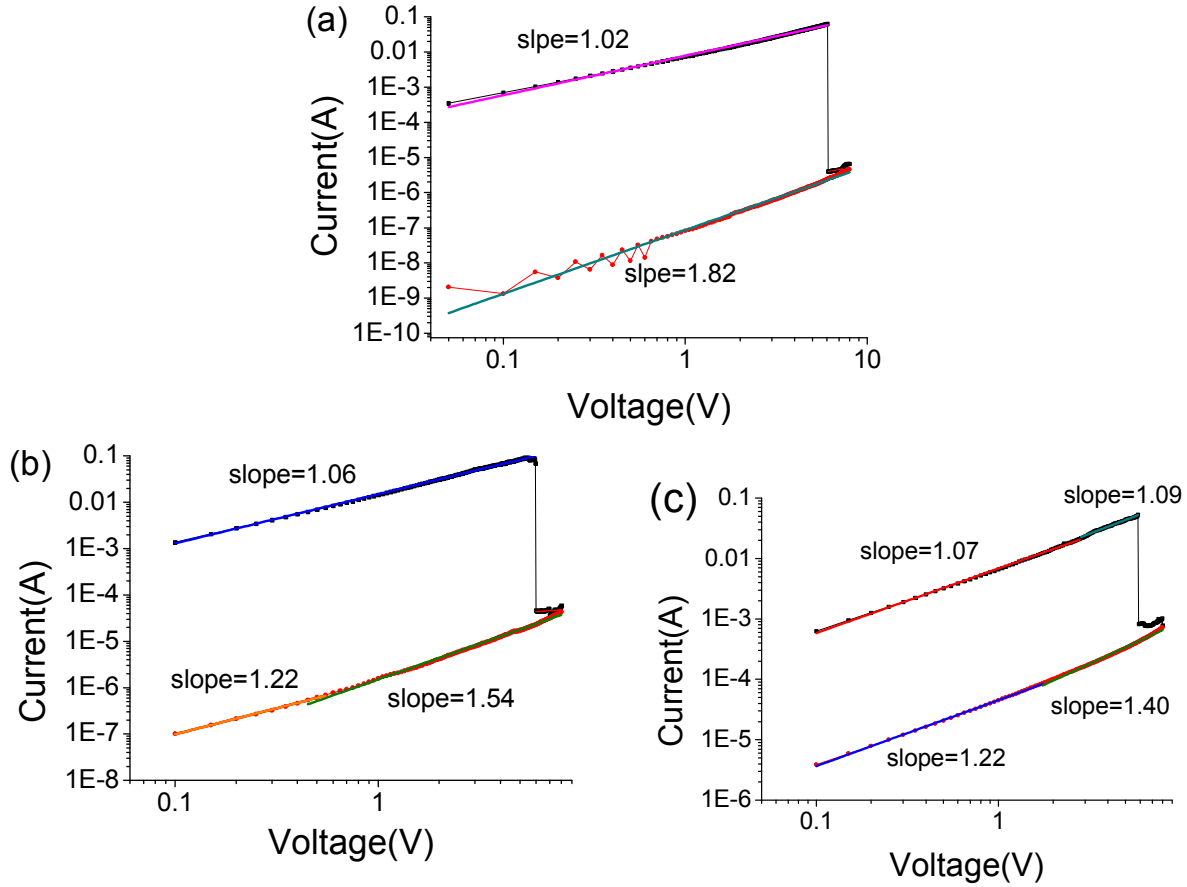

Fig. 13 Linear fitting and corresponding slopes for the *I-V* curves of ITO/PEDOT: PSS+SWCNTs/Al devices based on (a) sample A, (b) sample B, (c) sample C.

It can be concluded from the above analysis that the conductive behaviors for ON state and OFF state are completely different. The high conductivity of ON state is due to a conductive pathway, while the worse conductivity of OFF state is more like a bulk effect, a homogenously distributed one. The bulk currents are characterized by an approximate V^{m+1} dependence, which might be due to SCLC with a shallow-trap distribution (m<1).[22] In addition, compared with that of high conductivity states, the slope is

larger for low conductivity state; meanwhile the range with the slope larger than 1 is much wider for low conductivity state. The variation of the slope in the low conductivity state indicates that there are more charge traps was added into the mixture of PEDOT: PSS+SWCNTs. The SWCNTs is more likely to serve as the electron trapping center and electron transporter.[10] Thus, the decrease of SWCNTs in some extent and charge traps induced by the SWCNTs increased the current of low conductivity state.[23] PEDOT is a p-doped chain ($PEDOT^+$) meaning that the charge transport is realized by holes. Upon applying a voltage to the electrode, electrons are injected into the composite film and trapped by the SWCNTs. The trapped electrons will induce a countering space-charge layer near the Al electrode.

Spin-casting of the PEDOT: PSS+SWCNTs composites on ITO substrates leads to a conductive network with three dimensional and random orientation of of SWCNTs in the PEDOT: PSS matrix. Thus, the device behavior associated with charge carrier trapping and inter-SWCNTs hopping will be directly dependent on the effective distance between neighboring SWCNTs or the SWCNTs content in the composite film. With SWCNTs content increased, the distance between isolated nanotubes is significantly reduced, when the effective distance is even smaller than the diameter of individual carbon nanotubes and is suitable for charge hopping among individual nanotubes, continuous conductive pathways will be formed. A larger number of electrons are transferred via the carrier pathways, resulting in less charge carriers being trapped before switching. And the higher SWCNTs content will provide a larger number of electron pathways throughout the entire composite film. However, when the distance compared to the diameter of individual carbon nanotubes is too large for charge hopping in the PEDOT: PSS composite, the formation of continuous electron pathways will be difficult.

For devices based on sample A, B, C, containing more SWCNTs, continuous electron pathways are probably formed in the bulk films arising from the close stacking of the carbon nanotubes. In the initial ON state, electrons do not have sufficient energy/mobility to escape from the trapping centers, and the big current is attributed to the conduction channels caused by the SWCNTs,[24,25] which similar to the formation of Al filament in the device of Al/poly(9-vinylcarbazole)/Al.[26] when external bias is applied, whatever the bias, the charges can flow through the continuous electron pathways and sustain the device in ON state. A large number of charges flow through the formed conduction pathways, and this process might produce an excess of heat. When the voltage bias exceeds a certain value, the number of injected charges will rise more than the capacity of the conduction pathways. The generated heat will cause rupture of the conduction channels formed in the switch-OFF process.[27] Once the conduction channels are broken due to Joule heating, these are difficult to reform or the rate of formation of filaments is much less than their rupture.[28] As a result, the Joule heating and the conduction channels ruptures caused by the current passing through the conduction pathways change the device irreversibly to a low conductance state. The PEDOT: PSS matrix surrounding the SWCNTs holds on to the trapped charge carriers and the charged state even after turning off the power supply. Therefore, the composite film remains in the low conductivity state, leading to the non-volatile nature of the bistable device. For devices based on sample D, containing less SWCNTs, the distances between isolated nanotubes are increased, the charge carrier transport along the electron pathways via inter-SWCNTs hopping becomes difficult, keeping the devices in low conductivity state.

4. Conclusions

In conclusion, the electrical conductance switching behavior and nonvolatile memory effects in PEDOT: PSS and SWCNTs composite thin films have been investigated. In addition, the ON/OFF state

current ratio can also be tuned by varying the doping level, or the SWCNTs content, in the composite films. The controllable electrical properties and nonvolatile electrical bistable switching effects in the composite films can be attributed to continuous conductive pathways caused by the SWCNTs during spin-casting of the PEDOT: PSS+SWCNTs composites on ITO substrates. Finally, the effect of single-wall carbon nanotubes (SWCNTs) doping level on electrical conductance switching behavior of ITO/(PEDOT: PSS+SWCNTs)/Al devices has been explored, and it is possible to change the ON/OFF state current ratio by changing the nanotube doping level in the composite.

Acknowledgements

The authors are grateful to the support of the National Science Foundation of China (Grant no. 61204127 and 21372067), doctoral Fund of Ministry of Education of China (20132301110001).

Notes and references

1 S. R. Forrest, Nature, 2004, 428, 911.
2 T. Oyamada, H. Tanaka, K. Matsushige, H. Sasabe and A. Adachi, Appl. Phys. Lett., 2003, 83, 1252.
3 J. Yang, F. Zeng, Z. S. Wang, C. Chen, G. Y. Wang, Y. S. Lin and F. Pan, J. Appl. Phys., 2011, 110, 114518.
4 J. Y. Huang and D. G. Ma, Appl. Phys. Lett., 2014, 105, 093303.
5 S. Moller, C. Perlov, W. Jackson, C. Taussig and S. R. Forrest, Nature, 2003, 426,166.
6 Z. S. Wang, F. Zeng, J. Yang, C. Chen and F. Pan, Appl. Mater. Interfaces, 2012, 4, 447.
7 G. Liu and Q. D. Ling, ACS nano, 2009, 3, 1929.
8 G. Liu, Q. D. Ling, E. T. Kang, K.G. Neoh and D. J. Liaw, J. Appl. Phys., 2007, 102, 024502.
9 W. T. Kim, J. H. Jung and T. W. King, Appl. Phys. Lett., 2009, 95, 022104.
10 J. A. Ávila-Nino, W. S. Machado, A. O. Sustaita, E. Segura-Cardenas, M. Reyes-Reyes, R. López-Sandoval and I. A. Hümmelgen, Org. Electron., 2012, 13, 2582.
11 J. A. Ávila-Nino, E. Segura-Cárdenas, A. O. Sustaita, I. Cruz-Cruz, R. López-Sandoval and M. Reyes-Reye., Mater. Sci. Eng. B, 2011, 176, 462.
12 S. ChandraKishore and A. Pandurangan. RSC Adv., 2014, 4, 9905.
13 S. F. Miao, Y. X. Zhu, Q. Bao, H. Li, N. J. Li, S. J. Ji, Q. F. Xu, J. M. Lu and L. H. Wang, J. Phys. Chem. C, 2014, 118, 2154.
14 A. D. Yu, T. Kurosawa, Y. H. Chou, K. Aoyagi, Y. Shoji, T. Higashihara, M. Ueda, C. L. Liu and W. C. Chen, ACS Appl. Mater. Interfaces, 2013, 5, 4921.
15 C. J. Chen, Y. C. Hu and G. S. Liou, Chem. Commun., 2013, 49, 2804.
16 M. A. Khan, U. S. Bhansali, D. Cha and H. N. Alshareef, Adv. Funct. Mater., 2013, 23, 2145.
17 Z. F. Wang, H. Zhang, Z. P. Wang, J. Zhang, X. M. Duan, J. K. Xu and Y. P. Wen, Food Chem., 2015, 180, 186.
18 H. Ling, J. Lu, S. Phua, H. Liu, L. Liu, Y. Huang, D. Mandler, P. S. Lee and X. H. Lu, J. Mat. Chem. A, 2014, 2, 2708.
19 L. H. Ai, C. Y. Zhang, F. Liao, Y. Wang, M. Li, L. Y. Meng, J. Jiang, J. Hazard. Mater., 2011, 198, 282.
20 A. Suresh, G. Krishnakumar and M. A. G. Namboothiry, Phys. Chem. Chem. Phys., 2014, 16, 13074.
21 D. I. Son, D. H. Park, W. K. Choi, S. H. Cho, W. T. Kim and T. W. Kim, Nanotechnology, 2009, 20, 195203.
22 T. J. Lee, S. Park, S. G. Hahm, D. M. Kim, K. Kim, J. Kim, W. Kwon, Y. Kim, T. Chang and M. Ree,

J. Phys. Chem. C, 2009, 113, 3855.
23 S. M. Islam, P. Banerji and S. Banerjee, Org. Electron., 2014, 15,144.
24 G. Liu, Q. D. Ling, E. Y. H. Teo, C. X. Zhu, D. S. H. Chan, K. G. Neoh and E. T. Kang, ACS nano, 2009, 3, 1929.
25 S. ChandraKishorea and A. Pandurangan, RSC Adv., 2014, 4, 9905.
26 S. Aswin, K. Govind, A. G. N. Manoj, Phys. Chem. Chem. Phys., 2014, 16, 13074.
27 W. B. Zhang, C. Wang, G. Liu, X. J. Zhu, X. X. Chen, L. Pan, H. W. Tan, W. H. Xue, Z. H. Ji, J. Wang, Y. Chen, R. W. Li, Chem. Commun., 2014, 50, 11856.
28 W. J. Joo, T. L. Choi, J. Lee, S. K. Lee, M. S. Jung, N. Kim, J. M. Kim, J. Phys. Chem. B, 2006, 110, 23812.